A Ten-Meter Ground-Station Telescope for Deep-Space Optical Communications: A Preliminary Design

M. Britcliffe,[1] D. Hoppe,[1] W. Roberts,[2] and N. Page[3]

This article describes a telescope design for a 10-m optical ground station for deep-space communications. The design for a direct-detection optical communications telescope differs dramatically from a telescope for imaging applications. In general, the requirements for optical manufacturing and tracking performance are much less stringent for direct detection of optical signals. The technical challenge is providing a design that will operate in the daytime/nighttime conditions required for a Deep Space Network tracking application. The design presented addresses these requirements. The design will provide higher performance at lower cost than existing designs.

I. Introduction

The primary differences between a deep-space optical communications telescope and an imaging telescope are the wave-front error and the telescope field-of-view (FOV) requirements. To provide the highest resolution, an imaging telescope requires that all the energy received from the source be focused into a near-diffraction-limited image. This requires that the wave front across the aperture be a small fraction (<1/10th) of a wavelength. The wave-front error specification requires nanometer-level manufacturing tolerances of the optical surfaces and positioning of the components. Small changes in temperature result in thermal-expansion-induced distortion of the optical surfaces and require that the mirrors be manufactured from expensive low-thermal-expansion glass.

A telescope intended for direct detection of optical signals has a dramatically different wave-front error requirement. The energy at the detector does not need to be diffraction limited. It is assumed that the signal from the spacecraft appears as a point source that is blurred into a spot determined by the atmosphere. The only requirement is energy be focused into an angular spot comparable to the atmospheric blur. The surface specifications become geometrical. Instead of specifying a wave-front error in units of length, the surface error is expressed as a slope error in radians. The required surface figure is easier to achieve and less expensive than for a diffraction-limited system.

---

[1] Communications Ground Systems Section.

[2] Communications Systems and Research Section.

[3] Interferometry Systems and Technology Section.

The research described in this publication was carried out by the Jet Propulsion Laboratory, California Institute of Technology, under a contract with the National Aeronautics and Space Administration.

Imaging telescopes normally require that the wave-front error be constant over a large field of view to image extended objects. The FOV requirement normally requires aspherical shaping of the optical surfaces, which increases the cost of manufacturing. The FOV requirement for an optical communications telescope is simply determined by the maximum pointing error expected in operation. A typical value for blind pointing accuracy of a 10-m telescope is 100 μrad or less. This is small compared to normal imaging telescopes. This small FOV requirement allows the use of a spherical optical primary mirror, which reduces the cost of manufacturing and simplifies the logistics of operation.

The other major difference between imaging telescopes and an optical communications telescope intended for operation in the Deep Space Network (DSN) is the requirement for daytime operation. Astronomical telescopes are almost never exposed to daylight. The domes are closed before sunrise and until after sunset. In many cases, direct illumination of the primary mirror is prohibited. The solar energy reflected off the primary will be directed to some area on the telescope or the enclosure that will cause damage or thermal deformation.

Stray light from the Sun affects the telescope performance in a number of ways. Sunlight scattered into the focal plane is the most serious effect. In addition, any energy that is dissipated on or around the telescope structure may result in thermal deformation and misalign the telescope. Solar heating of the air in the optical path increases the atmospheric blurring or "dome seeing." Daytime operation also requires special attention to the cleanliness of the optical surfaces. Airborne contaminants settling on the optical surfaces will scatter sunlight into the optical path. Solar heating of structures will misalign the telescope.

Another challenge to operating an optical telescope in a changing thermal and gravity environment is pointing the telescope and maintaining the alignment of the optical system. This design uses an active pointing and alignment system. The system controls the telescope pointing, segment alignment, and focus adjustment using the signal from the spacecraft.

II. High-Level Requirements and Assumptions

The assumptions used to formulate this design are a departure from previous work. The high-level system requirements that led to the design chosen are shown below:

(1) Receive-only capability: The telescope will provide a receive-only capability. It is assumed that if an uplink is required a separate telescope will be used.

(2) Wavelength: The wavelength of operation (receive) is assumed to be 800 to 1550 nm (nominally 1060 nm).

(3) Diameter: The collecting area of the telescope will be equivalent to a 10-m circular aperture. The 10-m size has been determined in previous studies.

(4) Direct-detection operation: The telescope will operate in an incoherent or direct-detection mode only.

(5) Ground-based operation: The telescope is designed for ground-based operation only. No effort has been made to make the telescope consistent with space-based operation. Design of a cost-effective ground-based telescope is in many ways in direct conflict with the design of a cost-effective, low-mass, space-based telescope.

(6) Tracking: The telescope and mount is designed to track at sidereal rates and also to track high Earth orbit (HEO) objects.

(7) Day/night operation: The telescope is capable of operation during both day and night to provide DSN-like coverage of missions. The requirement for daytime operation is unique to DSN optical communications.

(8) Sun–Earth–probe (SEP) angle: The telescope is capable of tracking within 10 deg of the Sun, while maintaining a stray-light level within 3 dB of that when pointed away from the Sun. Tracking to within 1 deg of the Sun is considered a goal. This requirement is also intended to supply DSN-like coverage of missions.

(9) Telescope field of view: The required FOV is driven by pointing considerations only. The size of the FOV must be larger than the coarse pointing accuracy of the telescope, which is assumed for the present to be 100 μrad. The quality of the spot generated over this FOV must be sufficient for obtaining the approximate location (centroid) that is used to update the telescope pointing. As the spot is moved toward the center of the FOV, the quality improves, but a high-quality, wide FOV is not required.

(10) Communication detectors: The design requires a maximum detector diameter of 1.0 mm.

(11) Atmospheric conditions: The telescope will employ no atmospheric correction, and hence both the atmospheric seeing and the finite optical quality of the telescope surfaces will affect the blur diameter. An optimum design of the telescope can be determined only if some values for atmospheric seeing are specified. In the past, Shaik [1] has assumed seeing (blur-diameter) values of 5 μrad for operation at night and 25 μrad for daytime operation. Ortiz, Sandusky, and Biswas [2] have sized detectors at approximately 10 μrad for operation at night and 100 μrad during the day. The values for seeing are site dependent and not well documented for daytime operation. For the present design, taking into account these past estimates, conservative values would be 5-μrad best cases and 100-μrad worst cases for the atmospheric contribution to blur diameter. The 100-μrad value is considered quite conservative.

III. Optical System Performance

The energy collected with a direct-detection telescope does not need to be "in phase" at the signal frequency as it does with a diffraction-limited telescope or microwave antenna. A segmented direct-detection telescope functions as an array of individual apertures (the segments) focused on a single detector.

The path-length error requirement can be considered as the time-delay difference allowable between the energy from the individual segments. The time-delay requirement is determined by the modulation frequency of the carrier from the optical source rather than the carrier itself. Modulation rates considered for DSN missions are lower than 1 GHz. To satisfy this requirement, the segment-to-segment path-length error needs only to be on the order of a few millimeters. The alignment requirements for the optical system are determined by the blur requirement at the focal plane.

In the absence of background light from the Sun or other sources, the performance of an optical communications telescope is determined primarily by the product of the aperture area and collection efficiency (the amount of signal incident on the aperture that reaches the communication detector). The background light from the nighttime sky is small.

In the case of daytime operation, the requirements change dramatically. The increase in background light from night to day is typically 80 dB. In daytime conditions, the telescope performance is driven by the amount of sunlight incident on the detector. The detector size is determined by the size of the blur circle. Blur circle or spot size is the angle subtended by a point source imaged at the focal plane. It determines the required field of view of the detector (not to be confused with the field of view of the telescope).

The background-light level increases proportionally to the solid angle of the sky seen by the detector. The result is the signal-to-noise ratio decreases roughly as the square of the blur diameter. The perfor-

mance of a typical Mars mission communications link would improve 7 dB by using a telescope with a 10-μrad blur circle instead of a 100-μrad blur circle [3].

The overall blur size of the optical telescope system is the rss of the telescope blur and the atmospheric blur. As noted above, the expected atmospheric blur is in the range of 5 to 25 μrad for normal operation.

Previous designs provided a blur circle closer to 100 μrad [1]. The blur was driven by the surface figure of an aspheric composite primary mirror. The design goal for this telescope is 10 μrad. The improvement in performance is largely due to using a glass primary mirror. A telescope system with a 10-μrad blur circle provides a good compromise in optical performance and technical risk. The 10-μrad goal is achievable. It is ten times the diffraction limit for a single 1-m segment. The Hobby–Ebberly Telescope (HET) 10-m telescope that uses a similar optical design routinely achieves 10-μrad blur diameters that include the atmosphere.

Another optical performance requirement is stray-light control. Light from the Sun and other sources can be scattered to the detector in a number of ways. Imperfections in the manufacturing of the optical surfaces causes scattering. Scattering from contamination from airborne particles settling on the surfaces is a major concern. Light from off axis can be reflected from the telescope structure or dome. Careful attention to optical baffling and stop design is required. Stray-light control is the single most demanding aspect of optical communications telescope design.

The stray-light performance of the telescope is best described by its bidirectional reflectance distribution function (BRDF). The BRDF is the scattered surface radiance ($W/m^2/sr$) in a particular scatter direction divided by the incident surface irradiance (W/m^2). The preliminary BRDF requirement for the telescope primary was determined to be 0.02 [4]. That calculation assumed a sky brightness that was uniform over the sky and did not include the increase in the sky brightness seen in a field of view that approaches the Sun. At 10 deg from the Sun and including solar elongation,[4] the required BRDF for the telescope system is 0.003. This is not a challenging BRDF specification for an optical surface. Typical BRDF values for telescope optical surfaces are parts in 10^{-5}.

IV. Optical System Design

Both a prime-focus and a Cassegrain optical configuration have been studied. Both systems use a 10-m-diameter spherical primary mirror with a 10-m focal length. The key design assumptions are shown in Table 1.

Table 1. Key design assumptions.

Parameter	Value
Aperture diameter	10 m
Focal ratio	Fast as possible
Bandpass	800 nm to 1550 nm
Telescope field of view	100 μrad ($\pm$50 μrad)
Corrector configuration	Simple as possible

[4] K. Shaik and M. Wilhelm, *Ground Based Advanced Technology Study (GBATS)*, JPL D-110000, Release 1 (internal document), Jet Propulsion Laboratory, Pasadena, California, p. 27, August 1994.

V. Prime-Focus Design

The prime-focus design is shown in Fig. 1. It consists of a 10-m f/1.0 segmented primary mirror and two smaller corrector mirrors near the focal plane. Light from the primary mirror goes through a 110-mm-diameter hole in the tertiary mirror to the secondary mirror that is located beyond the primary paraxial focus. The tertiary mirror is placed near the caustic minimum and is located in the obscuration shadow of the secondary–tertiary assembly so that there is no additional loss of collecting aperture.

Because of the complexity of this design, the optical performance was studied in detail. A ray trace of the corrector assembly is shown in Fig. 2. The prescription for the optical surfaces is given in Table 2.

In this design, the secondary and tertiary mirrors are both aspheric, the tertiary departing particularly severely from the best-fitting sphere. Development and testing of this element, therefore, will be costly, but will be more than offset by the savings in structure, housing, and primary-mirror development afforded by the spherical primary mirror.

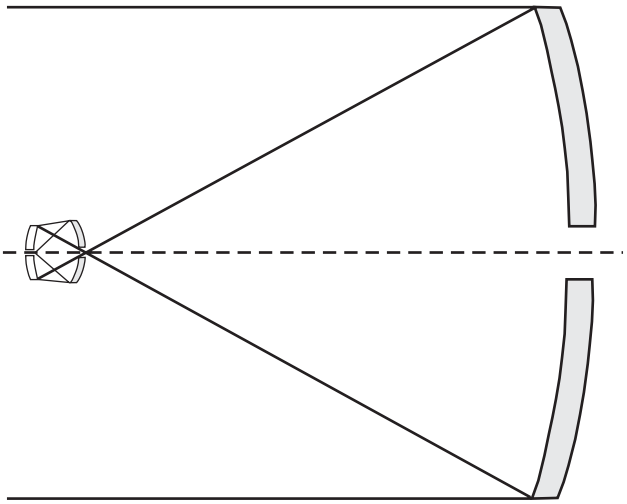

Fig. 1. Prime-focus design layout.

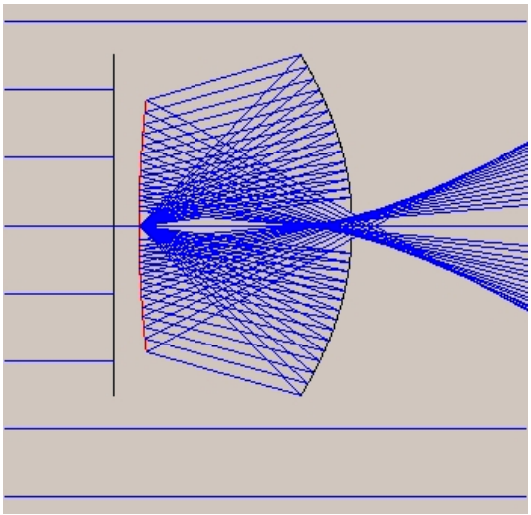

Fig. 2. Prime-focus corrector assembly.

Table 2. Prime-focus optical prescription.

Component	Conic constant	Curvature radius, mm	Diameter, mm	Spacing, mm
Primary mirror	Spherical	−20,000	10,000	10,690.477
Secondary mirror	−3.917437	4,709.772	1,100	922.37
Tertiary mirror	−0.889225	−1,241.807	1,477	922.37

The source footprint is seen in Fig. 3, in which point sources on axis and at 18 μrad, 35 μrad, and 50 μrad are shown. The spots from the off-axis sources suffer from a significant degree of coma; however, almost all of the light from any of these sources will fall on a 0.5-mm-diameter detector. This allows the system to work in high-turbulence conditions without an adaptive optics system to correct for atmospheric seeing. Furthermore, the spot quality is adequate for identifying the acquired source and guiding it to the center of the detector.

An initial tolerance study was performed on this design to evaluate the manufacturing and alignment tolerances required for the system. The various tolerance limits are shown in Table 3. In this table, the tolerance value is listed for each of the parameters, and the spot size at the tolerance value for that parameter alone is evaluated. For example, if the radius of curvature of the primary mirror is actually 20,001 mm rather than the nominal 20,000 mm, the spot size increases to 36 μm from its nominal value of 10 μm.

The most stringent tolerance must be placed on the conic constant of the tertiary mirror in order to correct the severe spherical aberration of the primary mirror. This will clearly be the most expensive element to produce and test. The conic constant on the secondary mirror is the next-most-critical item, but the tolerance here is 100 times less severe.

A Monte Carlo analysis was performed, perturbing each of the tolerance parameters listed in Table 3 by a value selected from a normal distribution centered on the nominal value with a standard deviation of the tolerance amount shown in Table 3. The location of the focus was allowed to vary in each case to compensate for the aggregate of the errors introduced by the tolerance perturbation. A histogram of the calculated spot sizes was generated based on 100 Monte Carlo trials. For comparison purposes,

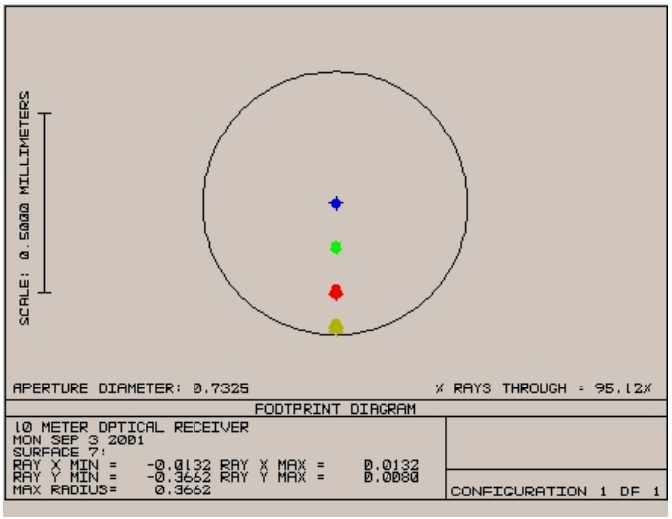

Fig. 3. Prime-focus design spot diagram.

Table 3. Prime-focus design tolerance limits.

Parameter	Nominal value	Units	Tolerance	Spot size, μm
Primary-mirror radius of curvature	20,000	mm	±1.0	36
Primary-mirror tilt—total indicator runout (TIR)	0	mm	±1.0	23
Primary-mirror surface irregularity	0	nm	±1.6	12
Primary–secondary distance	10,690.49	mm	±0.5	32
Secondary-mirror radius of curvature	4709.772	mm	±1.0	10
Secondary-mirror tilt—TIR	0	mm	±0.1	38
Secondary-mirror conic constant	−3.91744	—	±0.1	70
Secondary-mirror decentration	0	mm	±0.1	12
Secondary–tertiary distance	922.370	mm	±0.5	50
Tertiary-mirror radius of curvature	−1241.81	mm	±0.1	16
Tertiary-mirror tilt—TIR	0	mm	±0.1	14
Tertiary-mirror conic constant	−0.88923	—	−0.001	99
Tertiary-mirror decentration	0	mm	±1.0	13
Tertiary-detector distance	922.370	mm	±0.5	50

this histogram was recalculated assuming atmospheric seeing conditions of 5 μrad and 15 μrad (expected values for night and day observing conditions) and is shown in Fig. 4. The results of this analysis show that the tolerance values established are strict enough that the blur size is dominated by the nighttime atmospheric conditions for 95 percent of the trials run. Since the telescope must operate under daytime conditions where seeing, thermal distortions, and background noise are expected to be significantly worse, it may be possible to relax the tolerances considered here.

The prime-focus design may have an advantage in stray-light rejection. The detector is pointed away from stray-light sources outside the field of view. All light entering the secondary–tertiary assembly and ultimately reaching the detector must pass through the small 110-mm-diameter hole in the tertiary mirror. The back of the mirror can be made reflective to reject off-axis light, rejecting all direct illumination outside of 12 mrad. Thus, only scattered light will be observed within the 1-deg solar-angle goal.

The entire secondary–tertiary assembly can be enclosed by placing a window at the center hole in the tertiary mirror. It may be possible to design the window to include a notch filter that acts as the first stage of spectral rejection of out-of-band radiation. By sealing the assembly in this way, particulate contamination and stray light can be effectively minimized.

This design has the advantage that there is an internal focus at which a field stop could be placed. It also has a pupil image at the second corrector mirror where a Lyot stop could be implemented. These two stops could help reduce scattered light considerably. The effectiveness of the Lyot stop may be questionable because it is located near a mirror surface.

There are some disadvantages associated with this design. First, the location of the detector high on the structure makes routine operation more difficult. All external interfaces must be supplied to the detector assembly here, necessitating running lines along the secondary support structure. Maintenance access to the detector is more difficult than in a Cassegrain design. The large numerical aperture of the light incident on the detector requires that the detector be sensitive over a larger angle of incidence. It may require that any narrowband filter placed at the detector be applied uniformly to a spherical surface concentric with the detector. While these additional efforts are not particularly difficult to achieve, they nevertheless do add complexity and cost.

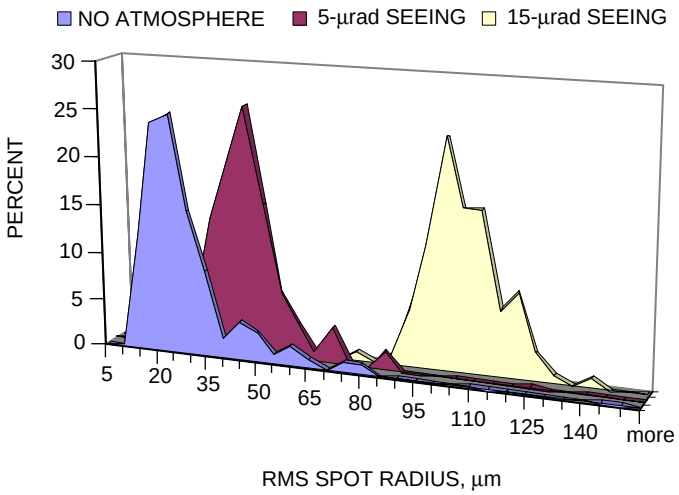

Fig. 4. Histogram of tolerance analysis.

VI. Cassegrain Design

The Cassegrain configuration is shown in Fig. 5. It consists of a 10-m-diameter f/1.0 segmented spherical primary mirror, an aspheric secondary mirror, and two small spherical refractive corrector elements near the focal plane.

The secondary mirror is a high-order asphere that would be fairly difficult to build. It deviates over 2.000 mm from the closest-fitting sphere. The corrector optics near the focal plane are small spherical lenses that should be easy to build.

The design has several advantages. First, it places the detector behind the primary mirror, where it can be accessed and easily supplied with necessary interfaces (cabling, etc.). Only the secondary mirror must be suspended in front of the primary mirror, reducing the weight and required stiffness of the support structure. The Cassegrain system provides nearly collimated regions of the beam appropriate for placement of narrowband notch filters for spectral rejection of out-of-band radiation. A tolerance study was not performed for the Cassegrain system and should be completed before this option is considered.

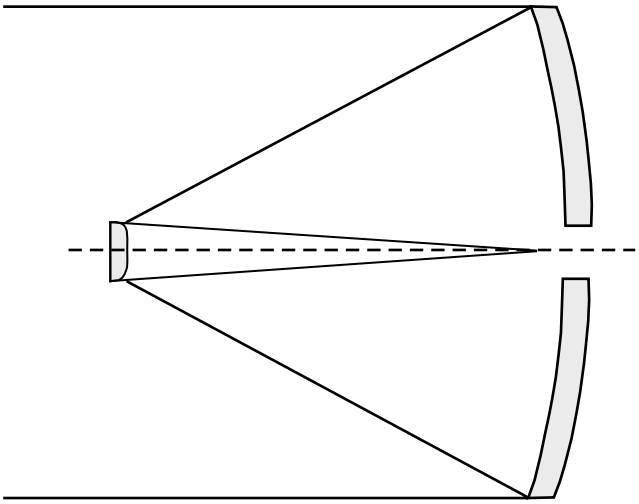

Fig. 5. Cassegrain design 1 layout.

VII. Other Optical Design Considerations

Both designs developed for the 10-m optical communications telescope show that there are theoretical optical designs that could yield the desired performance. There are advantages and disadvantages to both approaches in terms of off-angle performance, stray-light rejection, complexity, and operational concerns. Both of these designs would be difficult to implement due to tight alignment tolerances and aspheric surfaces that would be difficult to fabricate. Because the alignment tolerances will be tight, an active alignment system will be required to maintain the desired performance.

The severity of the aspheric surfaces in each design will make them difficult to build. Some work will be required to determine a suitable test setup for each aspheric optical element. These test setups may require the design and fabrication of special tooling, such as a null lens test optic.

The central obstruction due to the two corrector mirrors in the prime-focus design is about the same as the obstruction due to the secondary mirror in the Cassegrain system. Baffling in both designs would result in a central obstruction of about 1.5 m. This would give an area obstruction of about 2.3 percent. The trade-off between the Cassegrain and prime-focus systems requires further study.

VIII. General Telescope Design

The design uses a lightweight glass primary mirror. The selection of the primary mirror type was studied earlier [4]. Glass provides the best optical performance at very low technical risk. Using a lightweight approach provides the best compromise between optical performance and reflector weight. The weight of the primary mirror has a direct effect on the complexity and cost of the mirror support structure and the telescope mount and gimbal.

Deep-space optical communication is in the development stage, and the specific requirements for the telescope detector electronics are still being developed. To allow maximum flexibility, the system is designed to allow operation with the receivers at the prime focus or in a Cassegrain configuration.

The system was designed with the shortest focal length practical. Using a short telescope minimizes structural complexity and reduces the cost of fabrication. The focal length also determines the size of the dome.

The telescope is mounted on a conventional elevation-over-azimuth mount. The mount is similar in configuration to the Keck telescope mount. Using a lightweight glass primary mirror will require a structure that supports only one-third the weight of the Keck. It may be possible to use a wheel-and-track azimuth bearing in place of the Keck hydrostatic design.

The use of an active pointing detection system requires the pointing and tracking accuracy of the mount to be ± 50 μrad (0.003 deg). DSN microwave antennas have demonstrated pointing accuracy comparable to this. Achieving this pointing accuracy with a 10-m telescope should not be challenging. The details of the mechanical design require further study.

The telescope is enclosed in an approximately 26-m geodesic dome with a dome opening that tracks with the telescope. Geodesic domes have been used on the HET telescopes and other similar applications. The advantages of using a dome in terms of stray-light rejection, mirror-contamination prevention, solar-heating control, and wind-disturbance rejection outweigh the cost of construction. A conceptual drawing of the telescope and dome is shown in Fig. 6.

IX. Stray-Light and Solar-Heating Control

Past designs have considered a number of novel solutions for Sun protection, including a Sun shield integrated on the telescope structure [2]. These options are expensive and risky. Concerns associated

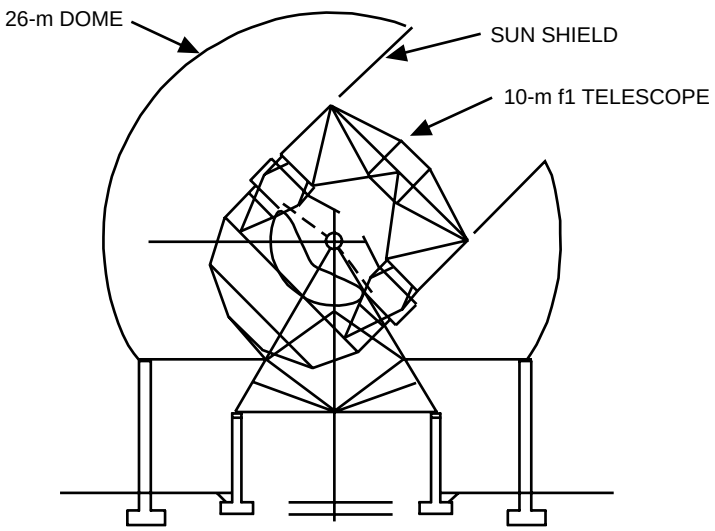

Fig. 6. Conceptual drawing of the telescope in the dome.

with attaching a Sun shield to the telescope structure include the increased structural complexity and cost to support the weight of the Sun shield and the problems of managing thermal radiation intercepted by the shield in the optical path.

In addition to proper stray-light design, including baffling and stops, the design uses a commercial geodesic dome. It is similar to the design used on the HET telescope, with the addition of a 10-m circular opening and Sun shield that is moved with the telescope. The HET dome is 26 m in diameter and costs less than one-sixth the cost of the Keck dome. This configuration provides inherent protection from the Sun. The Sun will be blocked from the main reflector for SEP angles larger than 30 deg.

The general solar-heating-control approach is to limit the area in direct view of the Sun and to minimize solar absorption. A 10-m circular aperture is potentially exposed to 100 kW of solar energy. If high-reflecting surfaces are used for the optical surfaces and structure exposed to the Sun, 90 percent of the energy will be reflected away from the telescope. The remaining 10 kW of solar energy absorbed can easily be handled by convection cooling from airflow supplied from the dome or by active temperature control.

The Sun shield attached to the dome could be an inflatable tube of aluminized Mylar built with proper baffling. The inflatable Sun shield has a number of advantages. First, there is no connection to the telescope structure. This will minimize any pointing disturbance from the dome motion. Since the tube is flexible, it minimizes the risk of the telescope striking the tube due to positioning-system failure. Pointing disturbances from wind buffeting caused by the tube also are eliminated. An inflatable structure of this size and complexity is easy and inexpensive to fabricate. Aluminized Mylar is available with high-reflectivity coatings and should not be a thermal problem. In cases where the tube baffle may need to be an absorbing surface, carbon-coated Mylar is highly absorptive. The inflatable approach also is easy to modify. It may be advantageous to ventilate the tube to provide airflow to minimize thermal changes in the optical path.

X. Optical Surface Contamination

Contamination of the primary mirror from airborne pollutants is a major problem. Giordano [5] studied the effect of contamination on mirror reflectivity at an astronomical telescope site. The results showed that the mirror reflectivity at that site would degrade from 8 to 18 percent per year as a result of airborne contaminants.

For daylight operation, the DSN telescope is actually more sensitive to scattered sunlight from contaminates than to small changes in the reflectivity. Assuming that the reduction in reflectivity noted above was due only to scattering off the particles and that the scattering was isotropic, the DSN telescope can tolerate only a 2 percent increase in reflectivity to exceed the BRDF limit where the scattered light from the contamination will degrade the signal-to-noise ratio by 3 dB.

The DSN telescope will require a built in CO_2 snow mirror-cleaning system. The dome will provide some inherent level of protection from contaminants. It may also be necessary to provide positive pressure ventilation with filtered air in an updraft configuration to minimize particle contamination and prevent condensation on the optical surfaces. The effects of contamination on the performance of the DSN telescope are critical and require further study.

XI. Active Panel Control System

Active panel control is expected to be critical for minimizing the size of the blur produced by the telescope. A number of segment-control algorithms are possible. In this section, a theoretical analysis of one of these systems is undertaken. The system under consideration is shown in Fig. 7. The ground station's focal plane contains both a high-speed communication detector and a slower charge-coupled device (CCD) array. Periodically each segment—in this case the ith segment—is tilted and focused on the CCD array. Assuming that there are approximately 100 segments in the primary, this removes 1 percent of the signal energy from the communication detector. The CCD array is used to centroid on the spot produced by the segment on the CCD array. Using this information, the segment is repointed precisely on the center of the communication detector. The next segment is now pointed on the CCD, and the process is repeated continuously throughout the track.

The most important factor in such a system is the available update rate. Thermal effects and nonrepeatable structural deformations will be the primary factors that cause pointing errors of the individual panels. The update rate must be sufficient to cover the bandwidth of these effects. Although a high update rate is favorable, a minimum integration time is required to obtain an accurate estimate of the centroid. Thus, there is a trade-off between update rate and centroid error. The performance of the system also depends critically on the strength of the spacecraft signal. Finally, the number of pixels used

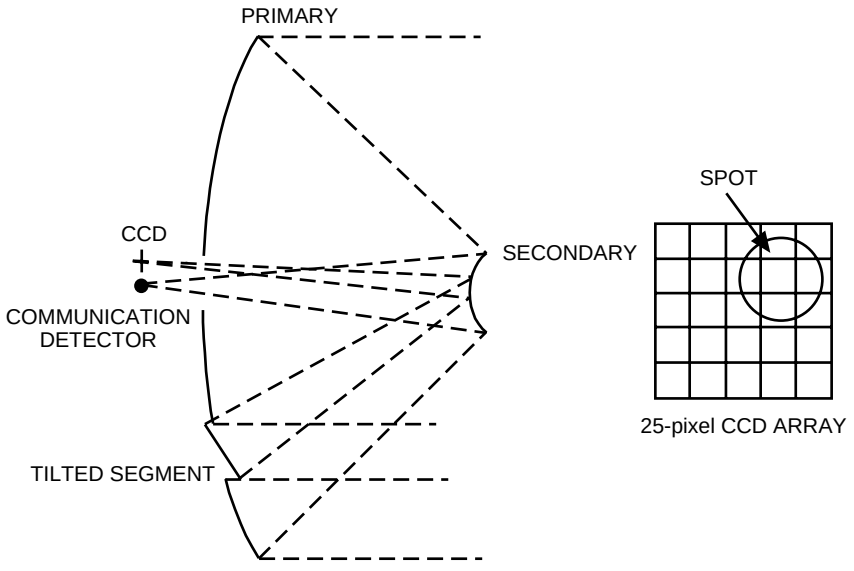

Fig. 7. Active panel control system.

to cover the spot also affects the performance of the system. For a small number of pixels, the resolution is poor, and saturation due to the background noise from the sky can be the limiting factor. For a large number of pixels, the small signal level per pixel and the noise of the pixel itself are the limiting factors.

Two spacecraft configurations—one suitable for a Mars mission, the other for Europa—were considered in this simulation. Their parameters are given in Table 4. The following spacecraft parameters were considered: average transmitter power, telescope diameter, Strehl ratio, telescope obscuration, optics efficiency, support-structure blockage, and pointing errors. The spacecraft range—1 au for Mars and 6 au for Europa—determines the space loss. Atmospheric transmission was assumed to be 0.43 for the simulations. The ground station was assumed to be 10 m in diameter with an efficiency of 0.8 for the primary and 0.58 for the relay optics. The daytime sky background radiation at 1.06 μm was assumed to be 1.0×10^{-3} W/(cm^2 μm steradian) [6]. The CCD parameters employed in the simulation are shown in Table 5 and should be considered "typical" values; no particular CCD was chosen for the study.

Table 4. Spacecraft parameters.

Parameter	Mars	Europa
Average transmitter power, W	1.00	3.00
Telescope diameter, m	0.10	0.30
Strehl ratio	0.86	0.86
Obscuration ratio efficiency	0.54	0.54
Optics efficiency	0.90	0.90
Support-structure efficiency	0.95	0.95
Pointing efficiency	0.63	0.63

Table 5. CCD parameters.

CCD parameter	Value
Quantum efficiency	0.5
Read noise, e/pixel	15
Dark current, e/s	1000
Pixel saturation, e	100,000

Figure 8 shows the centroid error normalized to the blur diameter versus integration time for 10-, 25-, 50-, and 100-μrad blur diameters for the hypothetical Mars mission. Figure 9 repeats the same information for the Europa parameters. Since the spacecraft parameters are scaled to give nearly the same power density at Earth for the two cases, the results are essentially identical. Read noise, sky background noise, and dark current have been included in the calculation of the centroid error. Saturation has not been considered in the figures but will be addressed later. It is assumed that the segment's spot is distributed over a 3×3 array of pixels, regardless of the size of the blur. In practice this would be accomplished through appropriate design of the reimaging optics. The effect of using more pixels will be discussed later. It is also assumed that there are 100 segments making up the primary mirror and all the light from the segment being aligned reaches the CCD array.

The figures illustrate that longer integration times result in less centroid error at the expense of a slower update rate. Smaller blur diameters allow the total amount of contaminating sky background to

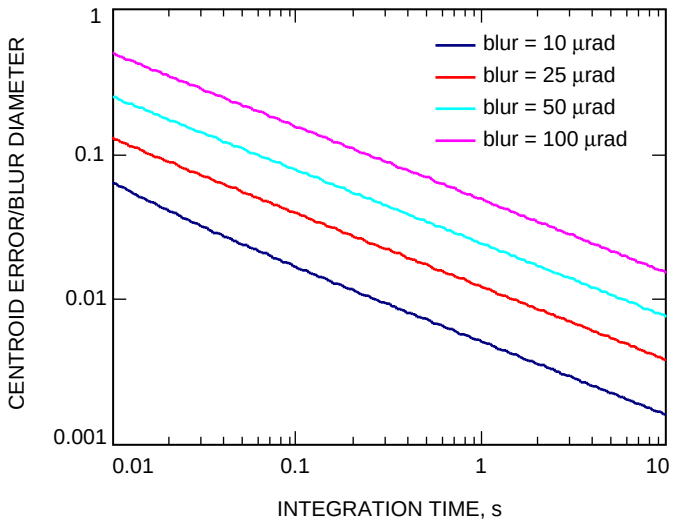

Fig. 8. Segment simulation (100 percent of a single panel's photons): Mars spacecraft package, 1 au.

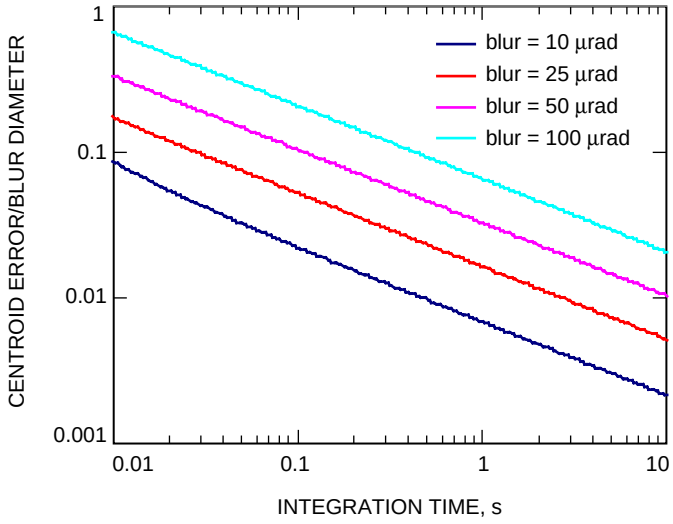

Fig. 9. Segment simulation (100 percent of a single panel's photons): Europa spacecraft package, 6 au.

be reduced. This results in a smaller normalized centroid error for smaller blur diameters, as illustrated in the figures. For the saturation value of 100,000 electrons given in Table 5, integration times would be limited to around 0.1 s for the 100-μrad blur, 0.02 s for the 50-μrad blur, 0.3 s for the 250-μrad blur, and 2 s for the 10-μrad blur. More complicated processing algorithms or a more careful choice of CCD can be used to alleviate this problem. An alternative is to spread the blur over more pixels. In this case, saturation occurs for longer integration times since less background light enters each pixel. Unfortunately, there is also less signal per pixel as well, and the two effects nearly balance. Table 6 shows the maximum allowable integration time due to saturation and the associated normalized centroid error versus number of pixels for blur diameters of 100 and 25 μrad. The table illustrates that smaller overall centroid errors can be achieved by using more pixels at the expense of update rate.

Table 6. Centroid error versus number of pixels.

Blur diameter, μrad	Pixels	T_{max}, s	Centroid error/ blur diameter
100	9	0.02	0.347
100	25	0.07	0.193
100	49	0.1	0.163
25	9	0.4	0.019
25	25	1.1	0.012
25	49	2.2	0.009

In order to determine the update rate available for a given blur diameter, we must select an allowable centroid error. Figure 10 shows detector coupling efficiency versus beam offset, assuming a Gaussian-shaped profile. For this plot, the beam diameter is defined to be the 1/e width of the beam. Curves for two different detector diameters are shown, one set to capture 90 percent of the energy in the beam when it is centered on the detector, the other for 85 percent capture. From these curves we see that losses can be kept to a few percent if the offset is maintained at 0.1 beam diameter or less.

Several conclusions can be drawn from the data in Figs. 8 and 9 and Table 6. For blur diameters of 50, 25, and 10 μrad, a 9-pixel array can provide sufficiently low centroid error, approximately 0.1, without saturation to achieve a loss in collection efficiency of less than a few percent. The corresponding integration times are 0.06 s for a blur diameter of 50 μrad, 0.02 s for a blur diameter of 25 μrad, and less than 0.01 s for a blur diameter of 10 μrad. Assuming 100 segments must be positioned, the overall update rates correspond to 6 s, 2 s, and less than 1 s. For the 100-μrad case, saturation occurs before the required centroid error can be achieved. Using 49 pixels, a relative error in the centroid of 0.16 can be achieved by integrating for 0.1 s without saturation. This relative error will still result in slightly less coupling efficiency than that quoted for the smaller blur diameters. The corresponding update period would be 10 s.

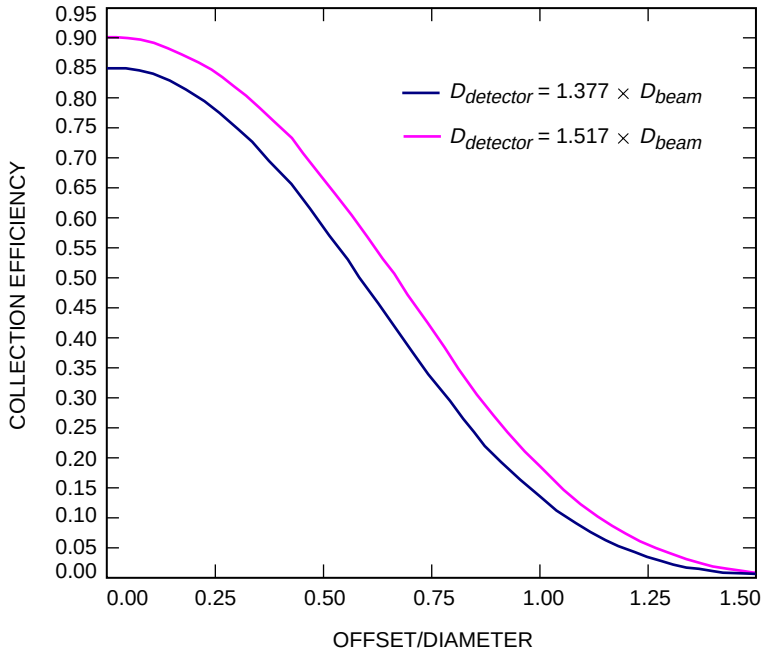

Fig. 10. Detector collection efficiency versus beam offset.

The results presented in this section indicate that a system using the spacecraft signal to point the individual segments is feasible. The achievable update rates should be sufficient to correct for thermal effects and structural effects with sufficiently long time constants. In practice the maximum update rate likely will be limited by the bandwidth of the segment position controller system.

It should be mentioned that the above analysis also applies to a real-time system for correcting the fine pointing of the ground station. In this case, a sample of the composite spot is directed to a CCD array and feedback is provided to a steering mirror to correct the overall pointing. Assuming the sample is coupled off at the 1 percent level, the above analysis applies directly to the pointing problem as well.

XII. Integrated Coaxial Pointing and the Communication Detector

Most of the acquisition and tracking systems considered to date use separate detectors for detecting the modulated carrier and determining the telescope pointing error. A schematic is shown in Fig. 11. A high-speed detector capable of detecting a modulation frequency of 300 MHz to 1 GHz is used for the communication detector. A beam splitter is used to reflect 10 percent of the energy to the pointing detector. A CCD array or a quad-cell position sensor is used to determine the pointing error.

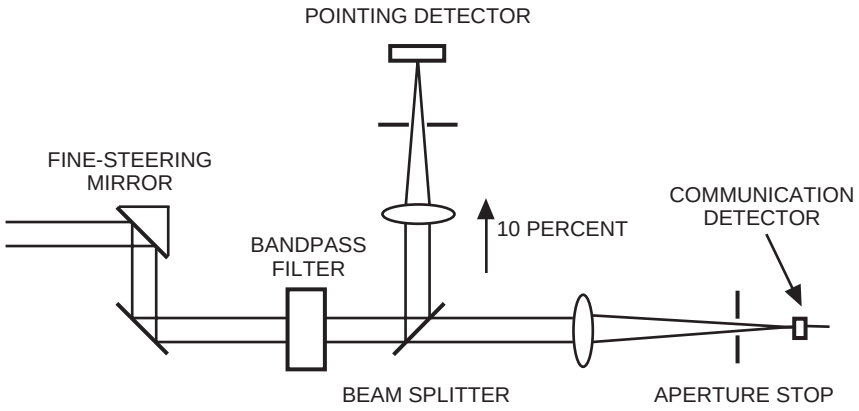

Fig. 11. Pointing detection system using a beam splitter.

This design has two disadvantages. First, 10 percent of the communication signal is lost in the beam splitter. Second, the performance of the pointing-error detector is limited by the signal-to-noise ratio provided by the signal available at the detector that is 10 dB below the main signal. Using this configuration for segment control will provide only 0.1 percent of the energy for segment alignment.

A new concept has been developed to solve this problem. The design uses a coaxial detector that integrates the communication and pointing detector at the focal plane. It consists of an inner disc containing the communication detector that is surrounded by an array detector used for pointing and segment alignment. A schematic is shown in Fig. 12.

The integrated detector takes advantage of the Gaussian energy distribution in the focal plane. By design, the communication detector is sized to receive 85 percent of the energy in the focal plane with the telescope pointed on bore sight. This is done to optimize the signal-to-noise ratio in the presence of background light. The region outside this circle contains 15 percent of the received signal distributed uniformly over a number of pixels for pointing detection. This is a fifty percent increase over the beam-splitter approach. For segment alignment, 1 percent of the energy is available per segment, as assumed in the previous segment-alignment analysis.

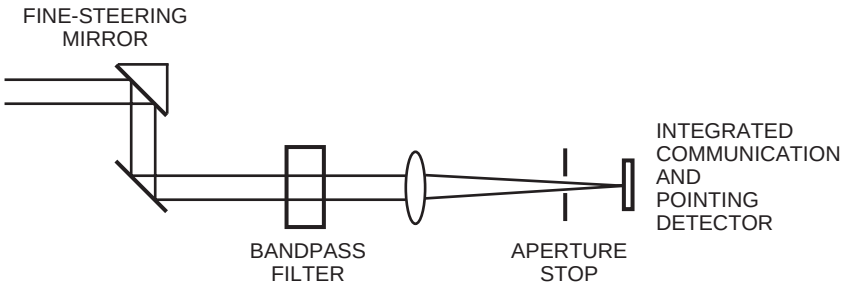

Fig. 12. Detection system using an integrated coaxial pointing and alignment detector.

Figure 13 shows the energy distribution on the coaxial detector in the focal plane. The communication detector shown is 0.1 mm in diameter. The pixel size shown for the pointing and alignment array is 10 μm. These dimensions were chosen as an example. The optimum pixel size and arrangement may be different.

Another advantage of this approach is that the energy available for pointing detection increases exponentially as the telescope moves off bore sight. This will allow the telescope pointing system to respond to large disturbances such as wind.

XIII. Conclusion and Recommendations

The telescope design described addresses the key technical challenges of implementing a system for DSN deep-space optical communications. The design goal for the blur diameter, which determines the detector field of view, is 10 μrad. This provides almost an order of magnitude better link performance than previous designs at lower cost.

Both a prime focus and a Cassegrain optical configuration that will work with the telescope have been developed. This provides flexibility for future development of optical communication technology. More

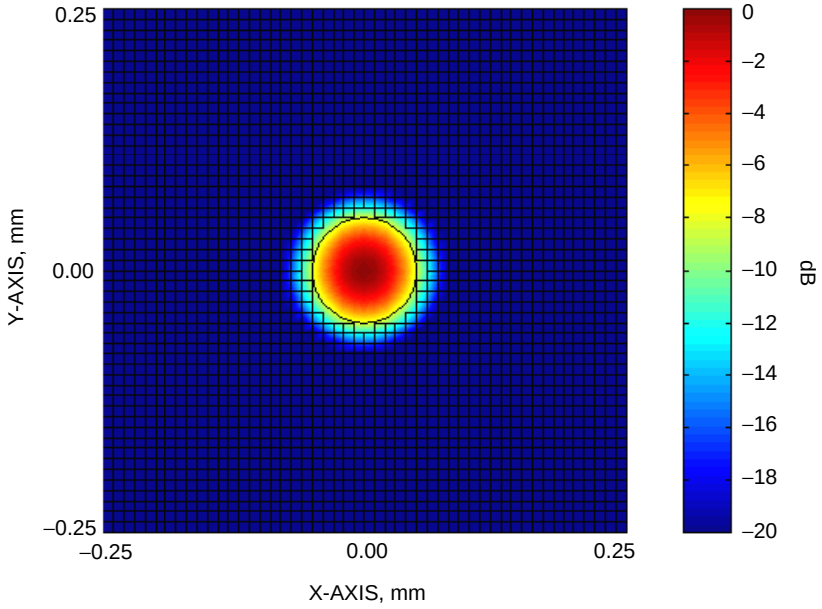

Fig. 13. Energy distribution on a coaxial communication and pointing detector.

work on the stray-light rejection problem and the actual detector system that will be used with the system need to be done to determine which is the best approach. Additional work on the performance of the Cassegrain is also required.

A critical component of the system is a pointing and segment-alignment system that will allow operation in a day/night environment. An alignment system that provides near-real-time alignment and pointing correction is described. The system uses the signal from the spacecraft and does not require guide stars.

Another challenge is providing environmental protection from contamination and solar heating of the telescope structure. The design presented uses a geodesic dome with an integral Sun shield that provides environmental protection at a minimum cost.

The biggest challenge to DSN optical communications is stray-light rejection. Future work should focus on studying the stray-light problem, including the effects of surface contamination. Future work should also address the mechanical design of the telescope mount and the support structure required.

Acknowledgment

Thanks to Shinhak Lee for helpful discussions regarding the signal-to-noise considerations of the active pointing and panel control system.

References

[1] K. Shaik, "Progress on Ten-Meter Optical Receiver Telescope," *Free Space Laser Communication Technologies IV*, SPIE vol. 1635, pp. 109–117, 1992.

[2] G. Ortiz, J. Sandusky, and A. Biswas, "Design of the Opto-Electronic Receiver for Deep Space Optical Communications," *Free Space Laser Communication Technologies XII*, SPIE vol. 3932, pp. 127–138, May 2000.

[3] J. R. Lesh and D. L. Robinson, "A Cost-Performance Model for Ground-Based Optical Communications Receiving Telescopes," *The Telecommunications and Data Acquisition Progress Report 42-87, July–September 1986*, Jet Propulsion Laboratory, Pasadena, California, pp. 56–64, November 15, 1986. http://tmo.jpl.nasa.gov/tmo/progress_report/42-87/87G.PDF

[4] M. J. Britcliffe and D. J. Hoppe, "Main-Reflector Manufacturing Technology for the Deep Space Optical Communications Ground Station," *The Telecommunications and Mission Operations Progress Report 42-145, January–March 2001*, Jet Propulsion Laboratory, Pasadena, California, pp. 1–10, May 15, 2001. http://tmo.jpl.nasa.gov/tmo/progress_report/42-145/145H.pdf

[5] P. Giordano, "Dust Contamination and In-Situ Cleaning of Ground-Based Telescope Optics: The VLT Approach," *Optical Telescope of Today and Tomorrow*, SPIE, vol. 2871, pp. 416–423, March 1997.

[6] R. Gagliardi and S. Karp, *Optical Communications*, second edition, New York: Wiley Inter-Science, p. 65, 1995.